Controlling thermodynamics of a quantum heat engine with modulated amplitude drivings

Sajal Kumar Giri ●

Department of Chemistry, Northwestern University, 2145 Sheridan Rd., Evanston, Illinois 60208, USA

Himangshu Prabal Goswami ●*

Department of Chemistry, Gauhati University, Jalukbari, Guwahati-781014, Assam, India

External driving of bath temperatures with a phase difference of a nonequilibrium quantum engine leads to the emergence of geometric effects on the thermodynamics. In this work we modulate the amplitude of the external driving protocols by introducing envelope functions and study the role of geometric effects on the flux, noise, and efficiency of a four-level driven quantum heat engine coupled with two thermal baths and a unimodal cavity. We observe that having a finite width of the modulation envelope introduces an additional control knob for studying the thermodynamics in the adiabatic limit. The optimization of the flux as well as the noise with respect to thermally induced quantum coherences becomes possible in the presence of geometric effects, which hitherto has not been possible with sinusoidal driving without an envelope. We also report the deviation of the slope and generation of an intercept in the standard expression for efficiency at maximum power as a function of Carnot efficiency in the presence of geometric effects under the amplitude modulation. Further, a recently developed universal bound on the efficiency obtained from the thermodynamic uncertainty relation is shown not to hold when a small width of the modulation envelope along with a large value of cavity temperature is maintained.

I. INTRODUCTION

Quantum heat engines (QHEs) have come a long way from the theoretically predicted Schulz-duBois engine [1] to experimentally realizable engines. Notable examples include Rb-based cold atomic setup [2], Li-based Fermi gas [3], diamond based N-vacancy centers [4], Paul-trapped Yb and Ca ion setups [5,6], and utilizing a proton's nuclear spin dissolved in ^{13}C-labeled CHCl$_3$ [7]. For the role of coherences in the quantum thermodynamic and transport properties, establishing the validity of nonequilibrium fluctuation theorems, thermodynamic uncertainity relationships (TURs) are now being investigated experimentally and compared with the results obtained from several theoretically established models [8–12]. Most of the theories are based on Markovian master equations and have seemed to agree pretty well with experimental observations [10,13]. The success of such master equations in understanding several steady-state properties of QHEs led to the widespread use of another class of master equations that theoretically predict dynamics of quantum systems where system parameters are modulated in time, usually called driven dynamics [14–16]. Toy models based on QHEs are often a common choice to study driven dynamics using adiabatic master equations [14,17]. In such driven systems, periodic or nonperiodic modulation of a system parameter (like energy, reservoir temperature, etc.) in an adiabatic fashion [18–23] has led to the theoretical prediction of exotic properties such as creating new phases of matter and loss

of tunneling. These are usually corroborated using Floquet theory coupled to adiabatic master equations [23–27]. Further, adiabatic master equations developed by modulating two system parameters have been shown to break nonequilibrium fluctuation theorems and TUR because of the emergence of geometric phaselike quantities [19,28–31]. Although driven QHEs (dQHEs) have not yet been experimentally realized, driven molecular junctions (the theory of which is akin to QHEs) have been experimentally studied where geometric phaselike effects were proven to exhibit nonstandard influence on transport properties as predicted by adiabatic master equations [32,33]. With such current experimental realization of QHEs and driven molecular junctions as well as observation of Floquet dynamics in driven spin systems using N-vacancy centers [34], it is not far off that driven QHE dynamics predicted by adiabatic master equations can be soon compared with experimental results.

There are several ways of driving the internal parameters of a dQHE. A particular example includes a stepwise sweep of the temperatures of the thermal reservoirs [35]. Such periodic driving protocols have led to the development of a quantum version of TUR signifying a trade-off between entropy production rate and signal-to-noise ratio [35]. Interestingly, over the past couple of years, several TUR have been developed in quantum engines [36–39]. In a previous study we have shown that such a trade-off is invalid in the presence of continuous driving of the temperatures of the two baths in a sinusoidal manner [29]. Violations of TUR due to nonsteady-state coherences have also been reported [40]. We have also shown how other thermodynamic quantities of a popular QHE model such as flux, noise, efficiency, power,
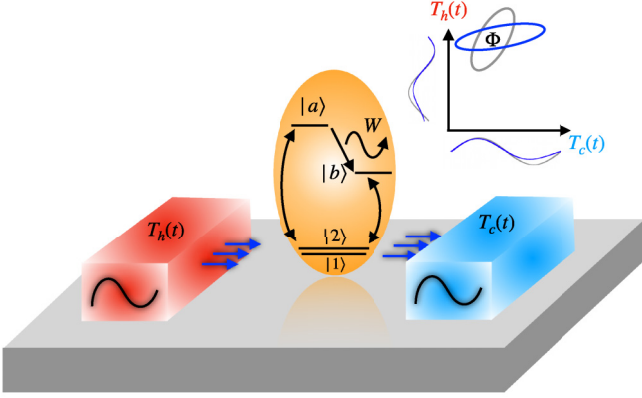
---

*hpg@gauhati.ac.in

024131-1

FIG. 1. Schematic plot of an amplitude-modulated driven four-level QHE. Two degenerate states $|1\rangle$ and $|2\rangle$ are coupled with higher energy states $|a\rangle$ and $|b\rangle$ through respective thermal baths. The state $|a\rangle$ is higher in energy than the state $|b\rangle$. Hot and cold bath temperatures are labeled as $T_h(t)$ and $T_c(t)$, respectively. States $|a\rangle$ and $|b\rangle$ are also coupled with a unimodal cavity. During the transition from $|a\rangle$ to $|b\rangle$ one photon is produced in the cavity with an energy equal to the energy difference between these states, which we treat as work done by the system denoted by W. Temperature amplitude shaping modifies the induced geometric phase Φ shown in the upper inset.

etc., are influenced by such drivings [29,41]. Notably, we showed that the universal linear slope of $1/2$ in the standard efficiency at maximum power (EMP) as a function of Carnot efficiency (η_c) no longer holds when there is a finite phase difference between the two continuous driving protocols [29]. A natural question is how the thermodynamic quantities would behave when the continuous driving is replaced by an amplitude-modulated driving (similar to a single-cycle pulse). Such pulse-induced dynamics have been studied previously in two-level thermal machines [42]. To keep things simple, we first focus on the adiabatic limit, where there are no sudden modulation- or pulse-induced dynamics in the engine, i.e., the driving timescale is well separated from the engine-evolution timescale. By considering two types of envelope functions, Gaussian and Lorentzian, we note some interesting observations and compare the results obtained with the known continuous sinusoidal driving, which is the limiting case with large envelope width.

This paper is organized as follows. In Sec. II we briefly introduce the model and discuss the basic underlying principles. In Sec. III we present our results and offer a discussion followed by the concluding remarks in Sec. IV.

II. AMPLITUDE-MODULATED DRIVEN QUANTUM HEAT ENGINE

We consider a four-level temperature driven quantum heat engine coupled with two thermal baths and a unimodal cavity (Fig. 1). This model has been studied in several works [29,43–46]. The theoretical framework has already been developed and discussed [29,41], and we refer to the Appendix for necessary details. The engine operates in such a way that two thermal baths at temperatures $T_h(t)$ and $T_c(t)$ are adiabatically driven externally. The driving protocol is cyclic whose

amplitude is being modulated in time thus shaping the envelope, which we refer to as *amplitude modulation*. We choose the following driving protocols:

$$T_c(t) = T_{c0} + A_i(t)\sin(\omega t), \tag{1}$$

$$T_h(t) = T_{h0} + A_i(t)\sin(\omega t + \phi), \tag{2}$$

where A_i is expressed as

$$A_S(t) = A_0, \tag{3}$$

$$A_G(t) = A_0 \exp\left(-(4\ln 2)\frac{t^2}{t_e^2}\right), \tag{4}$$

$$A_L(t) = A_0 \frac{[t_e/2]^2}{t^2 + [t_e/2]^2}, \tag{5}$$

with $i \in (S, G, L)$. Here t_e is termed as envelope duration and $A_i(t)$ is the envelope type such that the subscript i represents the type of envelope: constant, Gaussian, or Lorentzian. Note that t_e represents the time window of the envelope function where the amplitude modulation is being carried out and is mathematically defined as the full width at half maximum (FWHM) for both Gaussian and Lorentzian envelopes. A_0, ω, and ϕ are amplitude, frequency, and phase difference between the driving protocols, respectively. The time period of the two-parameter cyclic modulation is defined as $t_p = 2\pi/\omega$ which generates the geometric effects during the entire driving protocol [29]. It is within this time period that we control the envelope with t_e. Since the geometric contribution increases linearly with the driving frequency we choose to keep t_p constant throughout. However, t_e turns out to be a more interesting parameter, and its effect is addressed below in detail. Here the cold (hot) bath temperature oscillates around $T_{c0}(T_{h0})$. Bath temperatures are periodically driven in time such that the $T_h(t) > T_c(t)$ condition is maintained throughout. Note that the geometric contributions get explicitly added to the engine's thermodynamic properties due to the periodic driving of the reservoir temperatures. It is finite only when the driving protocols are phase different (which is introduced as a phase difference ϕ) [41]. Although we can observe driven dynamics when $\phi = 0$, geometric contributions change the driven dynamics if and only if $\phi \neq 0$. In this QHE, the exact analytical nature of the relationship between geometric effects and ϕ is not known, and so we resort to numerics to gain insights into its role on the thermodynamics. Throughout the text, whenever we refer to the phrase *in the presence of geometric contributions*, we mean $\phi \neq 0$ in the driving protocols. The central quantity of interest in this work is the effect of geometric contributions on the thermodynamics of the QHE. The work done by the engine W is quantified as energy flow (in the form of photon) into the cavity during the transition from $|a\rangle$ to $|b\rangle$. The hot and cold reservoirs induce coherence in the reduced system density matrix, and they are denoted as p_h and p_c, respectively [47]. Through the amplitude modulation in the driving protocols, the additional parameter FWHM (or envelope duration), t_e, allows us to control the overall geometric contributions to the thermodynamics of the QHE. In the next sections, we focus on the thermodynamic quantities as a function of the control parameters, *viz.*, envelope duration, t_e, and the hot bath-induced coherence parameter, p_h.
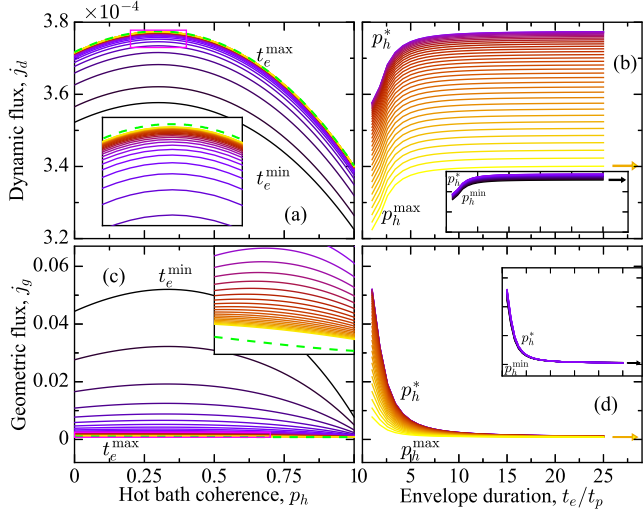
FIG. 2. Graphical representation of the dynamic (a, b) and geometric (c, d) fluxes as a function of p_h (left) for different t_e values ($t_e^{\min} = t_p$, $t_e^{\max} = 25t_p$) and as a function of t_e (right) for different p_h values ($p_h^{\min} = 0$, $p_h^{\max} = 1$) for a Gaussian envelope $A_G(t)$. (a) Dynamic flux j_d is optimized with p_h at various t_e. t_e increases from bottom to top. (b) j_d as a function of a dimensionless envelope duration, t_e/t_p (see text for interpretation). (c) Optimization of geometric flux j_g at finite envelope widths. t_e decreases from bottom to top. Inset shows dashed line where optimization is not possible for the sinusoidal driving. (d) Decrease in j_g with t_e. Arrows in (b) and (d) indicate fluxes for a sinusoidal driving for maximum (yellow) and minimum (black) p_h values, and p_h^* is the optimized p_h for dynamic flux. Here $T_{c0} = 1.0$, $T_{h0} = 1.67$, $T_l = 2$, $E_1 = E_2 = 0.1$, $E_b = 0.4$, $E_a = 1.5$, $A_0 = 0.01$, $\omega = 2500$, $p_c = 0.3$, $r = 0.1$, $g = 40$, $\tau = 0.01$, and $\phi = \pi/2$. Atomic units are used throughout.

III. RESULTS AND DISCUSSION

A. Flux and noise

The net photon flux exchanged between the engine and cavity is a fluctuating quantity. Both the flux (j) and the noise or fluctuations (n) in photon exchange are measurable quantities and are composed of additive dynamic (subscript d) and geometric parts (subscript g) given by [41]

$$j = j_d + j_g, \tag{6}$$

$$n = n_d + n_g. \tag{7}$$

The quantities j_d (j_g) are the first-order dynamic (geometric) cumulants, and $n_d(n_g)$ are the second-order dynamic (geometric) cumulants which can be obtained directly from a cumulant-generating function described in the Appendix [Eq. (A3) and Eq. (A4)]. Figures 2 and 3 display the behavior of the flux and the noise, respectively, for the Gaussian envelope $A_G(t)$ [Eq. (4)] as a function of the hot bath-induced coherence p_h and envelope duration t_e in the unit of driving period t_p. It is interesting to notice the two extremal limits of the envelope functions, $A_G(t)$: (1) it reduces to a Dirac delta function, $A_0\delta(t)$ when $t_e \to 0$ and (2) in the other limit, $t_e \to \infty$, it transforms into sinusoidal driving, $A_S(t)$ [Eq. (3)].
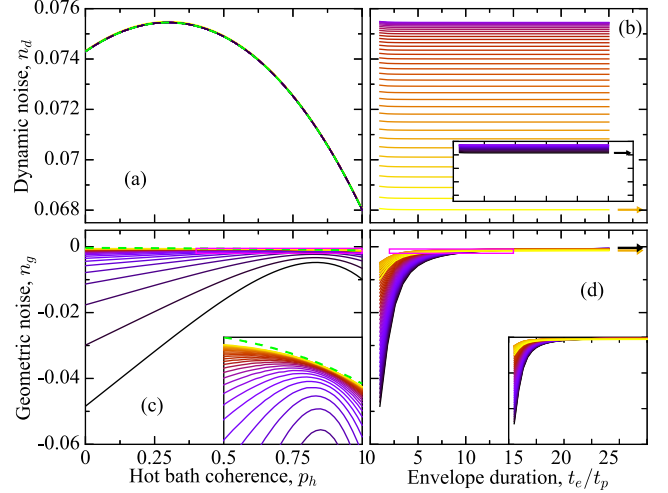

FIG. 3. Dynamic (a, b) and geometric (c, d) noise for the driving with Gaussian envelope $A_G(t)$. The same color code is used as in Fig. 2. Green dashed lines are for the $A_S(t)$ envelope. (a) Optimization of the dynamic noise n_d as a function of hot bath coherence p_h for different values of t_e. Note that the envelope shape and duration has no effect on the optimization of the dynamic noise. (b) n_d as a function of envelope duration t_e for different values of p_h. From the blue to the yellow curves, p_h increases from $p_h = p_h^*$ to $p_h = 1$, and in the inset from black to blue p_h increases from $p_h = 0$ to $p_h = p_h^*$. (c) Optimization of the geometric noise n_g as a function of p_h for different values of t_e. Note that, although the geometric noise is negative, the total noise (sum of geometric and dynamic noise) is always positive, preserving the definition of the second cumulant. (d) Behavior of n_g with t_e for different values of p_h. In (b) and (d), black and yellow arrows represent the noise for the $A_S(t)$ envelope for $p_h = 0$ and $p_h = 1$, respectively.

In Fig. 2(a) j_d is plotted as a function of p_h for increasing t_e (bottom to top), and in Fig. 2(b) j_d is plotted against t_e for the range $0 \leqslant p_h \leqslant 1$. For all t_e values, j_d is optimizable with p_h, and the optimized p_h (p_h^*) is independent of t_e. j_d increases with t_e rapidly and then saturates to the sinusoidal driving [green dashed line in Fig. 2(a) with the arrows representing two different p_h values in Fig. 2(b)]. In Fig. 2(b) one clearly sees that the saturation threshold (the minimum value of t_e for the saturation) does not depend on p_h.

In Figs. 2(c) and 2(d), the geometric flux j_g is evaluated for the full range of p_h and t_e. As a function of p_h, j_g shows a remarkably different behavior than j_d, where we see optimization of the flux when t_e is smaller than a critical value. This is in contrast to what we observed earlier for sinusoidal driving, where we reported that optimization was not possible in the case of j_g as a function of p_h [29]. But upon envelope modulation, the optimization is possible below a critical t_e value. Contrary to the dynamic flux optimization, the optimal value of hot bath-induced coherence, p_h^*, at which we see the optimized geometric flux, is dependent on t_e. Further, j_g decreases as t_e increases and eventually approaches sinusoidal driving [green dashed line in Fig. 2(c) and arrows for the two different p_h values in Fig. 2(d)], which is complementary to the behavior of j_d.

The dynamic (n_d) and geometric (n_g) noise are displayed in Fig. 3 spanning the full range of p_h and t_p. In Fig. 3(a) we
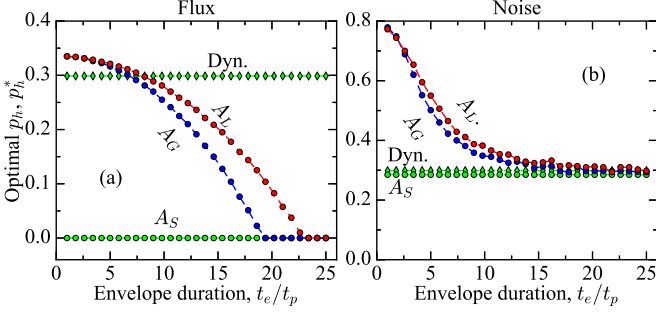
FIG. 4. Variation of the optimal value of hot bath coherence p_h^*, as a function of envelope duration t_e in the unit of t_p for (a) flux and (b) noise. Total (dynamic + geometric) contributions are plotted along with the dynamic contribution (green diamond points) for three different envelopes: sinusoidal [green circles, Eq. (3)], Gaussian [blue circles, Eq. (4)], and Lorentzian [red circles, Eq. (5)]. Dynamic contribution does not depend on the envelope shape.

have shown that n_d is optimizable as a function of p_h for all values of t_e. Interestingly, we observe that the optimization of flux and noise occurs at the same value of p_h^*, $p_h^* = 0.3$ for the considered parameters. Further, the noise does not change with t_e and remains constant as the sinusoidal driving [green dashed line in Fig. 3(a) and arrows in Fig. 3(b)]. This behavior is also reflected in Fig. 3(b), where n_d for all values of p_h is shown to be independent of t_e. In Fig. 3(c) the geometric noise is calculated with respect to p_h (t_e increases from bottom to top). As t_e is decreased, n_g starts exhibiting an optimizable character. This behavior is similar to that of j_g. The difference is that, where j_g decreases, n_d increases with t_e, as shown in Fig. 3(d). In Fig. 3(d) we see that n_g sharply increases at lower values of t_e and saturates to the value obtained from sinusoidal driving [green dashed line in Fig. 3(c) and arrows in Fig. 3(d)] at different evaluated values of p_h.

In Fig. 4 we show the dependence of the envelope duration t_e on the optimal coherence p_h^* for the dynamic and total (dynamic + geometric) flux (j) as well as noise (n). In Fig. 4(a) the line at $p_h^* = 0.3$ (green diamonds) represents the j_d value and highlights the independence of p_h^* on the envelope shape and duration t_e. The line at $p_h^* = 0$ (green circles) represents the total flux when there is a sinusoidal driving. In the latter case, the total flux is dominated by the geometric contribution, and the optimized values of flux occur at $p_h = 0$, as known previously [29]. In the presence of modulated drivings (both Gaussian and Lorentzian), unlike the sinusoidal driving, the value of p_h^* smoothly decreases from a large value as we keep increasing t_e depending on the shape of the envelope. In Fig. 4(b) for the dynamic noise (green diamonds) the optimal value of p_h^* is independent of envelope shape and duration and p_h^* does not depend on t_e for the sinusoidal driving (similar to what was observed for the flux). The p_h^* value is, however, larger in the presence of amplitude modulation (Lorentzian or Gaussian) and gradually meets the sinusoidal driving as t_e increases again depending on the shape of the envelope.

B. Efficiency and uncertainty relationship

The work done by the engine is the stimulated emission of photons into a unimodal cavity coupled to the higher energy
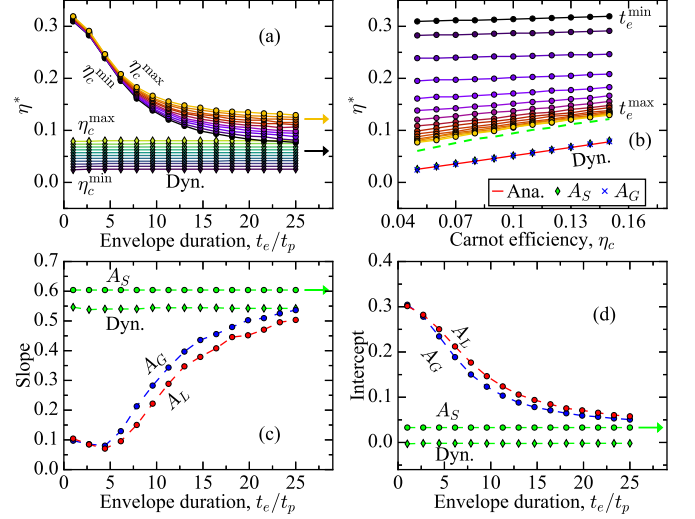

FIG. 5. (a) Efficiency at maximum power η^* for dynamic (blue to yellow lines) and total (black to orange lines) contributions as a function of envelope duration t_e for increasing Carnot efficiency η_c from bottom to top ($\eta_c^{\min} = 0.04$ and $\eta_c^{\max} = 0.15$). Black and yellow arrows represent the values of η^* for the $A_S(t)$ envelope [Eq. (3)] for minimum and maximum values of considered η_c, respectively. (b) η^* as function of η_c for different values of t_e (black to yellow lines t_e increases). Green dashed line is for the $A_S(t)$ envelope [Eq. (3)]. Red line is obeying the standard equation $\eta^* = \eta_c/2$ [Eq. (11)]. Green diamond and blue cross points represent dynamic part of the $A_S(t)$ [Eq. (3)] and $A_G(t)$ [Eq. (4)] envelopes, respectively. (c) Slopes for the lines in panel (b). Green diamond points represent the dynamic contribution (does not depend on the envelope shape). Green, blue, and red circles are for total (dynamic + geometric) contributions for the $A_S(t)$ [Eq. (3)], $A_G(t)$ [Eq. (4)], and $A_L(t)$ [Eq. (5)] envelopes, respectively. (d) Same as panel (c) but intercepts for the lines in panel (b).

states of the engine which is given by

$$W = E_a - E_b + \frac{1}{t_p} \ln \frac{(1 + n_l)}{n_l} \int_0^{t_p} dt' T_c(t'). \quad (8)$$

n_l is the cavity Bose-Einstein occupation factor expressed as $n_l = 1/\{\exp[(E_a - E_b)/T_l] - 1\}$ with T_l being the temperature of the cavity [44]. The power can be expressed as

$$P = W(j_d + j_g) = W j. \quad (9)$$

The efficiency of the system can be written as $\eta = W/(E_a - E_1)$. From the time integral in the definition of W, Eq. (8), it can be seen that η depends on both t_e and t_p. However, there is no geometric contribution on η, and hence we do not look into it. We instead choose to focus on the more interesting quantity, η^* (EMP), since the dependence of t_e, t_p and the geometric effects are directly observable through the two-parameter driving protocol in the definition of power in Eq. (9). η^* can be obtained by optimizing η with respect to an engine parameter (here we choose E_b). The efficiency at maximum power (EMP) depends on both t_p and t_e. Due to the chosen nature of the driving protocol, t_p is rendered fixed. Since the envelope duration, t_e, is a control parameter, addressing its role on EMP is more important, and we choose to numerically investigate its effect on η^*. In Fig. 5(a) we

show the behavior of η^* with respect to t_e for the range $0.05 < \eta_c < 0.15$ (bottom to top). The total η^* (with both dynamic and geometric contributions) is maximum (> 0.3) when the envelope duration is minimum ($t_e = t_p$). η^* non-linearly decreases as t_e increases and eventually saturates to the value obtained from sinusoidal drivings at large t_e. The lower set of curves (parallel lines) correspond to η^* values, when there are no geometric contributions (evaluated by using $\phi = 0$). In this scenario, η^* does not depend on t_e anymore, since $j_g = 0$ resulting in flat lines.

A popular analytical expression for η^*, called the Curzon-Ahlborn efficiency at maximum power, can be written in terms of the Carnot efficiency, η_c, given by

$$\eta^* = 1 - \sqrt{1 - \eta_c} \tag{10}$$

$$= \frac{1}{2}\eta_c, \text{ near equilibrium.} \tag{11}$$

We evaluate η^* as a function of t_e of the modulated driving and compare the results with Eq. (11). The linear coefficient, $1/2$ in Eq. (11), has been claimed to be universal [48,49], which we showed was violated in the presence of geometric effects [29] with sinusoidal drivings. In Fig. 5(b), we show that η^* linearly increases with η_c, but the slope is $1/2$ only when geometric contributions are absent (this holds for dynamic, green diamond, and blue cross points). Further, t_e has no effect on the slope under the same conditions. However, in the presence of geometric effects, this slope of $1/2$ is not maintained anymore. Note that $\eta^* < \eta_c$ is true only for a nondriven engine. In our case, the two-parameter driving protocol creates extra geometric pumping allowing $\eta^* > \eta_c$. Moreover, introduction of amplitude modulation even allows $\eta^* \gg \eta_c$ as can be seen in Fig. 5(b). The behavior of the slope and intercept in the presence of geometric effects is shown graphically in Figs. 5(c) and 5(d), respectively. The slope decreases, reaches a minimum, and then gradually increases and saturates at the respective values obtained for sinusoidal case, for both Gaussian and Lorentzian drivings. Note that, as per Eq. (11), there is no intercept in η^* as a function of η_c. In the presence of geometric effects, an intercept is introduced in the standard expression because of the driven dynamics. This intercept nonlinearly decreases with t_e and approaches the value obtained from sinusoidal drivings.

Efficiency, being one of the most characteristic quantities of engines, is often intensively investigated to gain deeper thermodynamic insights. During the last two years, with respect to QHE, several interesting bounds on efficiency have been proposed [36], especially derived from TUR [36]. One of such bounds on the efficiency of QHEs is given by [35]

$$\gamma/\eta \geqslant 1, \text{ with } \gamma = \frac{\eta_c P}{T_c \dot{\Sigma} + P}, \tag{12}$$

where $\dot{\Sigma}$ represents the rate of entropy production and has been claimed to be a direct result of TUR in quantum systems [38]. The average entropy production is given by $\dot{\Sigma} = j\mathcal{A}$, where $\mathcal{A}$ is the thermodynamic affinity [50]. Using an established TUR of the type $\mathcal{A}n/j \geqslant 2k_B$ [50], it is straightforward to recast Eq. (12) to ($k_B \to 1$)

$$\gamma/\eta \geqslant 1, \text{ with } \gamma = \frac{\eta_c P}{P + T_c \mathcal{A} j}. \tag{13}$$

It is natural to see the validity of Eq. (13) in the presence of geometric effects as well as other engine parameters. Although other TURs have been proposed, these involve evaluation of constancies and power fluctuations [36–39] and cannot be addressed within the currently employed formalism, and we leave it as a future prospect.

In our engine the thermodynamic affinity is known and is given by $\mathcal{A} = \ln \frac{\widetilde{n}_l \int_0^{t_p} dt'[1+n_c(t')]n_h(t')}{n_l \int_0^{t_p} dt' n_c(t')[1+n_h(t')]}$ [41]. We numerically evaluate γ and η in Eq. (13) and plot γ/η as a function of envelope duration, t_e, in Fig. 6, evaluated at different cavity temperatures T_l and coherence values p_h. In Figs. 6(a), 6(c), and 6(e), there are no geometric contributions (only dynamic, $\phi = 0$), and the inequality $\gamma/\eta > 1$ is always maintained irrespective of any engine parameters. From the insets, we show that γ/η changes its order with respect to p_h as T_l increases [Figs. 6(a)–6(e)]. Most interestingly, in the presence of geometric contribution [Figs. 6(b), 6(d), and 6(f)], by suitably selecting T_l and t_e we report a region where the inequality (13) does not hold. This happens at very small values of t_e and large values of T_l where we observe that $\gamma/\eta < 1$. As t_e increases, the driving approaches the value obtained from sinusoidal drivings where the inequality is recovered. Therefore, the inequality condition is broken only in the presence of geometric effects introduced due to amplitude modulation. If the amplitude modulation is absent, the inequality holds.

IV. CONCLUSION

In this work, we chose to drive the two temperatures of the thermal reservoirs of a quantum heat engine with protocols where the driving amplitude is being modulated in the adiabatic limit introducing envelope functions. With such amplitude modulation, we reported the optimization of the geometric flux with respect to quantum coherences for a finite envelope duration, which is otherwise not possible with simple sinusoidal drivings. Further, we also optimized the dynamic as well as the geometric noise, and this optimization is independent of envelope duration for the former one, whereas for the latter one the optimization point is envelope duration dependent. The optimal value of coherence decreases as the envelope duration is increased depending on the shape of the envelope. Another interesting thermodynamics quantity, the efficiency at maximum power (EMP), decreases nonlinearly with the envelope duration. In the presence of both geometric effects and modulated driving with envelope, the slope and intercept rise, which deviate from the standard linear expression for EMP in terms of Carnot efficiency in an intricate manner depending on the shape and duration of the envelope. Further, universal bounds on efficiency based on uncertainty relationships do not hold when geometric effects are employed via amplitude modulation with shorter envelope duration and larger cavity temperatures.

ACKNOWLEDGMENTS

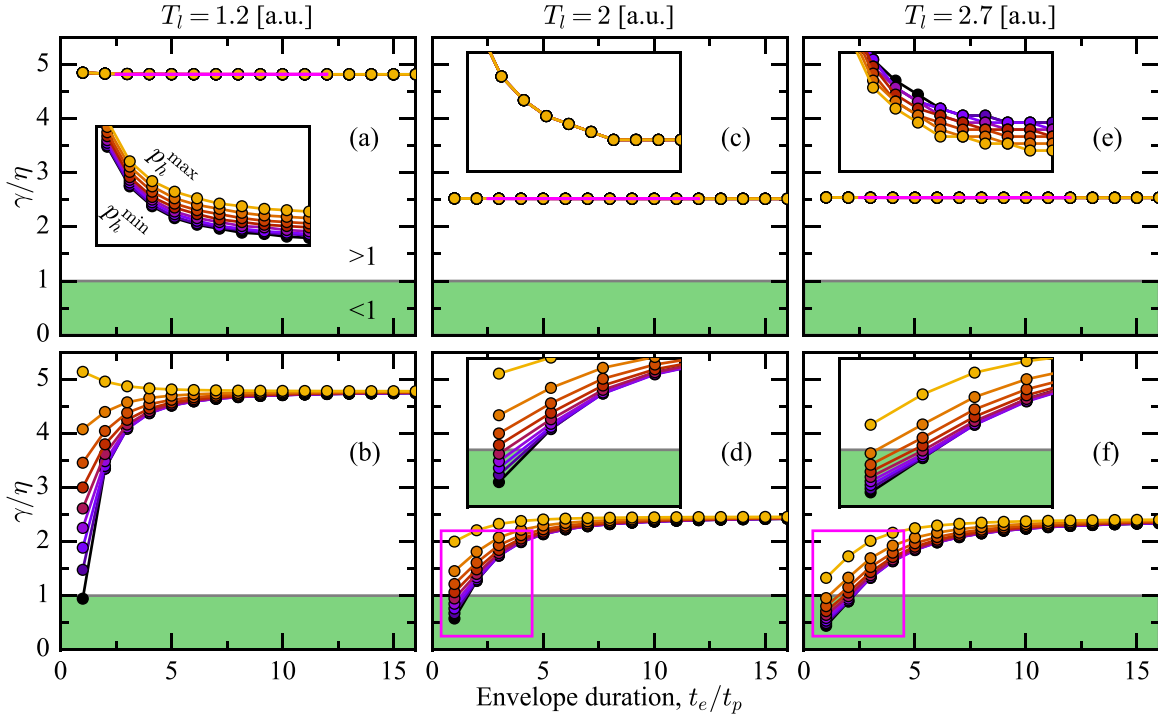FIG. 6. γ/η for dynamic (top) and total (bottom) contributions as a function of envelope duration t_e for (a, b) $T_l = 1.2$, (c, d) $T_l = 2$, and (e, f) $T_l = 2.7$, in the range $0 \leqslant p_h \leqslant 1$.

APPENDIX: METHOD OF FULL COUNTING STATISTICS

The full theoretical description of the QHE and the associated formalism can be found in many earlier works [29,41,43,45,46]. Here we present only the necessary details and omit the existing reports to avoid repetition. The QHE is composed of two degenerate quantum states $|1\rangle$ and $|2\rangle$, with the same symmetry (therefore with a forbidden transition between them) and coupled to two thermal baths. Two energy states $|a\rangle$ and $|b\rangle$ belonging to different symmetry and therefore with allowed transition are coupled to the hot and the cold bath, respectively. The state $|a\rangle$ is higher in energy than the state $|b\rangle$. $|1\rangle$, $|2\rangle$, $|b\rangle$, and $|a\rangle$ states correspond to the energies of E_1, E_2, E_b, and E_a, respectively. States $|a\rangle$ and $|b\rangle$ are also coupled to a unimodal cavity, and the strength of the coupling is denoted by g. The total Hamiltonian is written as $\hat{H}_T = \hat{H}_0 + \hat{V}_{sb} + \hat{V}_{sc}$, where

$$\hat{H}_0 = \sum_{v=1,2,a,b} E_v |v\rangle\langle v| + \sum_{k \in h,c} \epsilon_k \hat{a}_k^\dagger \hat{a}_k + \epsilon_l \hat{a}_l^\dagger \hat{a}_l,$$

$$\hat{V}_{sb} = \sum_{k \in h,c} \sum_{i=1,2} \sum_{x=a,b} r_{ik} \hat{a}_k |x\rangle\langle i| + \text{H.c},$$

$$\hat{V}_{sc} = g\hat{a}_l^\dagger |b\rangle\langle a| + \text{H.c.} \tag{A1}$$

In the above equation, E_v, ϵ_k, and ϵ_l are the energy of the system's vth level, kth mode of the thermal reservoirs, and unimodal cavity, respectively. r_{ik} is the system-reservoir coupling of the ith state with the kth mode of the reservoirs. Thermal baths are modeled as harmonic modes with $\hat{a}^\dagger(\hat{a})$ being the bosonic creation (annihilation) operators. There is a heat flow from the hot bath to the cold bath in a nonlinear fashion. Also, there is a radiative decay channel originating from the transition $|a\rangle \rightarrow |b\rangle$.

À propos of the theoretical full counting statistical (FCS) formalism in the Liouville space, presented in our earlier works [29,41], a reduced density vector in the Liouville space is composed of four coupled populations and a coherence given by $|\rho(\lambda, t)\rangle = \{\rho_{11}, \rho_{22}, \rho_{aa}, \rho_{bb}, \text{Re}(\rho_{12})\}$, with $i = 1, 2, a, b$, which denotes the system's many-body states and $\text{Re}(\rho_{12})$ is the thermally induced coherence between states $|1\rangle$ and $|2\rangle$. An adiabatic Markovian quantum master equation approach combined with a standard generating function technique allows us to evaluate the statistics of photons exchanged between the engine and the cavity as per the equation $\dot{\rho}(\lambda, t)\rangle = \check{\mathcal{L}}(\lambda, t)|\rho(\lambda, t)\rangle$, where λ is a field that counts the number of photons exchanged between the system and the cavity. $\check{\mathcal{L}}(\lambda, t)$ is the adiabatic effective evolution Liouvillian superoperator within the Markov approximation, given by

$$\check{\mathcal{L}}(\lambda, t) = \begin{pmatrix} n_1(t) & 0 & r_{1h}\tilde{n}_h(t) & r_{1c}\tilde{n}_c(t) & y(t) \\ 0 & n_2(t) & r_{2h}\tilde{n}_h(t) & r_{2c}\tilde{n}_c(t) & y(t) \\ r_{1h}n_h(t) & r_{2h}n_h(t) & -g^2\tilde{n}_l - 2r_h\tilde{n}_h(t) & g^2 n_l e^{-\lambda} & 2r_h p_h n_h(t) \\ r_{1c}n_c(t) & r_{2c}n_c(t) & g^2\tilde{n}_l e^{\lambda} & -g^2 n_l - 2r_c\tilde{n}_c(t) & 2r_c p_c n_c(t) \\ \frac{y(t)}{2} & \frac{y(t)}{2} & r_h p_h \tilde{n}_h(t) & r_c p_c \tilde{n}_c(t) & -n(t) \end{pmatrix}. \tag{A2}$$

In the above equation $n_i(t) = -[r_{ic}n_c(t) + r_{ih}n_h(t)]$ with $i = 1, 2$, $r_c = r_{1c} + r_{2c}$, $r_h = r_{1h} + r_{2h}$, $y(t) = -r_c n_c(t) p_c - r_h n_h(t) p_h$, $\tilde{n}_c(t) = n_c(t) + 1$, $n(t) = (r_{1h} + r_{2h})n_h(t)/2 + (r_{1c} + r_{2c})n_c(t)/2 + \tau$, $\tilde{n}_h(t) = n_h(t) + 1$, $\tilde{n}_l = 1 + n_l$, and τ is an environmental dephasing parameter. In this study we have considered equal system-reservoir coupling denoted by r. The explicit form of $n_c(t)$ and $n_h(t)$ can be expressed as $n_c(t) = 1/\{\exp[(E_b - E_1)/k_B T_c(t)] - 1\}$, $n_h(t) = 1/\{\exp[(E_a - E_1)/k_B T_h(t)] - 1\}$. p_h and p_c are the quantum coherence control parameters associated with the hot and cold baths, respectively. These quantify the orientation of the transition dipoles during heat absorption (emission) from (to) the hot (cold) bath.

The statistics of q (number of photons exchanged between the system and the cavity) is obtained from moment-generating function, which is expressed as $G(\lambda, t) = \sum_q e^{\lambda q} P(q, t)$ where $P(q, t)$ is the probability distribution function corresponding to q net photons in the cavity within a measurement window, t. Within the currently employed FCS formalism, it can be shown that $\dot{G}(\lambda, t) = \langle \check{\mathbf{1}} | \check{\mathcal{L}}(\lambda, t) | \rho(\lambda, t) \rangle$ with $\langle \check{\mathbf{1}} | = \{1, 1, 1, 1, 0\}$ [51,52]. With the help of Eq. (A2), one can obtain geometric contributions from the scaled cumulant-generating function given by $S(\lambda) = \lim_{t \to \infty}(1/t) \ln[\langle \check{\mathbf{1}} | \exp[\check{\mathcal{L}}(\lambda, t)t] | \rho(\lambda, t) \rangle]$. $S(\lambda)$ is separable into dynamic and geometric parts additively, $S(\lambda, t) =$

$S_d(\lambda, t) + S_g(\lambda, t)$:

$$S_d(\lambda) = \frac{1}{t_p} \int_0^{t_p} dt' \zeta_o(\lambda, t'), \tag{A3}$$

$$S_g(\lambda) = -\frac{1}{t_p} \int_0^{t_p} \langle L_o(\lambda, t) | \dot{R}_o(\lambda, t) \rangle \, dt. \tag{A4}$$

In the above equation, $S_d(\lambda)$ and $S_g(\lambda)$ represent the dynamic and geometric cumulant-generating functions, respectively. $|R_o(\lambda, t)\rangle$ and $\langle L_o(\lambda, t)|$ are the instantaneous right and left eigenvectors of $\check{\mathcal{L}}(\lambda, t)$ with an instantaneous long-time dominating eigenvalue, $\zeta_o(\lambda, t)$. Note that analytical expressions for both $S_d(\lambda)$ and $S_g(\lambda)$ cannot be derived for four-level dQHE. The cumulant-generating function is analytically known only for two-level systems [31,33] within the Markov limits. In systems with a large number of states, analytical expressions have not been reported since the geometric contributions involve calculation of both the left and right eigenvectors of the Hamiltonian. The nth-order fluctuations [cumulants of $S(\lambda)$] can be calculated as

$$C_d^{(i)} = \partial_\lambda^i S_d(\lambda)|_{\lambda=0}, \tag{A5}$$

$$C_g^{(i)} = \partial_\lambda^i S_g(\lambda)|_{\lambda=0}. \tag{A6}$$

When $i = 1$, we get the dynamic (geometric) flux, $j_d(j_g)$, and when $i = 2$, we obtain the dynamic (geometric) noise, $n_d(n_g)$, which are numerically evaluated.

[1] H. Scovil and E. Schulz-DuBois, Phys. Rev. Lett. **2**, 262 (1959).

[2] Y. Zou, Y. Jiang, Y. Mei, X. Guo, and S. Du, Phys. Rev. Lett. **119**, 050602 (2017).

[3] J.-P. Brantut, C. Grenier, J. Meineke, D. Stadler, S. Krinner, C. Kollath, T. Esslinger, and A. Georges, Science **342**, 713 (2013).

[4] J. Klatzow, J. N. Becker, P. M. Ledingham, C. Weinzetl, K. T. Kaczmarek, D. J. Saunders, J. Nunn, I. A. Walmsley, R. Uzdin, and E. Poem, Phys. Rev. Lett. **122**, 110601 (2019).

[5] G. Maslennikov, S. Ding, R. Hablützel, J. Gan, A. Roulet, S. Nimmrichter, J. Dai, V. Scarani, and D. Matsukevich, Nat. Commun. **10**, 202 (2019).

[6] J. Roßnagel, S. T. Dawkins, K. N. Tolazzi, O. Abah, E. Lutz, F. Schmidt-Kaler, and K. Singer, Science **352**, 325 (2016).

[7] J. P. S. Peterson, T. B. Batalhao, M. Herrera, A. M. Souza, R. S. Sarthour, I. S. Oliveira, and R. M. Serra, Phys. Rev. Lett. **123**, 240601 (2019).

[8] N. M. Myers, O. Abah, and S. Deffner, AVS Quantum Sci. **4**, 027101 (2022)

[9] G. Benenti, G. Casati, K. Saito, and R. S. Whitney, Phys. Rep. **694**, 1 (2017).

[10] S. Pal, T. S. Mahesh, and B. K. Agarwalla, Phys. Rev. A **100**, 042119 (2019).

[11] D. Mayer, F. Schmidt, S. Haupt, Q. Bouton, D. Adam, T. Lausch, E. Lutz, and A. Widera, Phys. Rev. Research **2**, 023245 (2020).

[12] J. Liu and D. Segal, Phys. Rev. E **103**, 032138 (2021).

[13] S. Hernández-Gómez, N. Staudenmaier, M. Campisi, and N. Fabbri, New J. Phys. **23**, 065004 (2021).

[14] K. Li, Y. Xiao, J. He, and J. Wang, arXiv:2202.06651 (2022).

[15] K. Brandner, M. Bauer, and U. Seifert, Phys. Rev. Lett. **119**, 170602 (2017).

[16] J. Liu, K. A. Jung, and D. Segal, Phys. Rev. Lett. **127**, 200602 (2021).

[17] B. Çakmak and Ö. E. Müstecaplioglu, Phys. Rev. E **99**, 032108 (2019).

[18] J. Tian, H. Liu, Y. Liu, P. Yang, R. Betzholz, R. S. Said, F. Jelezko, and J. Cai, Phys. Rev. A **102**, 043707 (2020).

[19] K. Takahashi, Y. Hino, K. Fujii, and H. Hayakawa, J. Stat. Phys. **181**, 2206 (2020).

[20] W. Niedenzu and G. Kurizki, New J. Phys. **20**, 113038 (2018).

[21] B. Bhandari, P. T. Alonso, F. Taddei, F. von Oppen, R. Fazio, and L. Arrachea, Phys. Rev. B **102**, 155407 (2020).

[22] J. Eglinton and K. Brandner, Phys. Rev. E **105**, L052102 (2022).

[23] S. Scopa, G. T. Landi, and D. Karevski, Phys. Rev. A **97**, 062121 (2018).

[24] T. Albash, S. Boixo, D. A. Lidar, and P. Zanardi, New J. Phys. **14**, 123016 (2012).

[25] B. Ye, F. Machado, and N. Y. Yao, Phys. Rev. Lett. **127**, 140603 (2021).

[26] S. Restrepo, J. Cerrillo, P. Strasberg, and G. Schaller, New J. Phys. **20**, 053063 (2018).

[27] R. Dann, A. Levy, and R. Kosloff, Phys. Rev. A **98**, 052129 (2018).

[28] Z. Wang, L. Wang, J. Chen, C. Wang, and J. Ren, Front. Phys. **17**, 1 (2022).

[29] S. K. Giri and H. P. Goswami, Phys. Rev. E **96**, 052129 (2017).

[30] T. Simons, D. Meidan, and A. Romito, Phys. Rev. B **102**, 245420 (2020).

[31] J. Ren, P. Hänggi, and B. Li, Phys. Rev. Lett. **104**, 170601 (2010).

[32] J. Gu, X.-G. Li, H.-P. Cheng, and X.-G. Zhang, J. Phys. Chem. C **122**, 1422 (2018).

[33] H. P. Goswami, B. K. Agarwalla, and U. Harbola, Phys. Rev. B **93**, 195441 (2016).

[34] Z. Shu, Y. Liu, Q. Cao, P. Yang, S. Zhang, M. B. Plenio, F. Jelezko, and J. Cai, Phys. Rev. Lett. **121**, 210501 (2018).

[35] H. J. D. Miller, M. H. Mohammady, M. Perarnau-Llobet, and G. Guarnieri, Phys. Rev. Lett. **126**, 210603 (2021).

[36] J. M. Horowitz and T. R. Gingrich, Nat. Phys. **16**, 15 (2020).

[37] P. Menczel, E. Loisa, K. Brandner, and C. Flindt, J. Phys. A: Math. Theor. **54**, 314002 (2021).

[38] T. Koyuk and U. Seifert, Phys. Rev. Lett. **125**, 260604 (2020).

[39] Y. Hasegawa, Phys. Rev. Lett. **126**, 010602 (2021).

[40] Alex Arash Sand Kalaee, A. Wacker, and P. P. Potts, Phys. Rev. E **104**, L012103 (2021).

[41] S. K. Giri and H. P. Goswami, Phys. Rev. E **99**, 022104 (2019).

[42] S. Mondal, S. Bhattacharjee, and A. Dutta, Phys. Rev. E **102**, 022140 (2020).

[43] M. O. Scully, K. R. Chapin, K. E. Dorfman, M. B. Kim, and A. Svidzinsky, Proc. Natl. Acad. Sci. USA **108**, 15097 (2011).

[44] H. P. Goswami and U. Harbola, Phys. Rev. A **88**, 013842 (2013).

[45] S. Rahav, U. Harbola, and S. Mukamel, Phys. Rev. A **86**, 043843 (2012).

[46] U. Harbola, S. Rahav, and S. Mukamel, EPL (Europhys. Lett.) **99**, 50005 (2012).

[47] A. A. Svidzinsky, K. E. Dorfman, and M. O. Scully, Coherent Optical Phenomena **1**, 7 (2012).

[48] C. Van den Broeck, Phys. Rev. Lett. **95**, 190602 (2005).

[49] M. Esposito, K. Lindenberg, and C. Van den Broeck, Phys. Rev. Lett. **102**, 130602 (2009).

[50] B. K. Agarwalla and D. Segal, Phys. Rev. B **98**, 155438 (2018).

[51] L. S. Levitov and M. Reznikov, Phys. Rev. B **70**, 115305 (2004).

[52] M. Esposito, U. Harbola, and S. Mukamel, Rev. Mod. Phys. **81**, 1665 (2009).